Valley-Polarized Quantum Anomalous Hall Effect in Ferrimagnetic Honeycomb Lattices

Jian Zhou, Qiang Sun, and Puru Jena

Phys. Rev. Lett. **119**, 046403 — Published 27 July 2017

DOI: 10.1103/PhysRevLett.119.046403

Valley-Polarized Quantum Anomalous Hall Effect in Ferrimagnetic Honeycomb Lattice

Jian Zhou[1,*], Qiang Sun[2,3,1], Puru Jena[1,†]

[1] *Physics Department, Virginia Commonwealth University, Richmond, VA 23284, USA*

[2] *Department of Materials Science and Engineering, College of Engineering, Peking University, Beijing 100871, People's Republic of China*

[3] *Center for Applied Physics and Technology, College of Engineering, Peking University, Beijing 100871, People's Republic of China*

Abstract

Valley-polarized quantum anomalous Hall effect (VP-QAHE), which combines valleytronics and topology in one material, is of significant fundamental and practical importance in condensed-matter physics and materials science. In previous model studies, VP-QAHE occurs under strong extrinsic Rashba spin-orbit coupling (SOC), which is an extrinsic effect. Here, using a low energy $k \cdot p$ model, we propose a different mechanism of VP-QAHE by introducing an intrinsic staggered magnetic exchange field and develop a general picture of valley dependent band inversion in honeycomb lattice. Using first-principles calculation, this new mechanism is further demonstrated in Co decorated In-triangle adlayer on a Si(111) surface. This system is equivalent to a ferrimagnetic honeycomb lattice, and the supported adlayer is experimentally more feasible in synthesis, thus exhibiting advantages over the existing studies based on Rashba SOC and free-standing sheets. The underlying physical mechanism is generally applicable, opening a new avenue for exploration of substrate supported VP-QAHE.

The electronic properties of semiconductors are governed by the nature of their valence and conduction bands. Novel physics does emerge when the extrema of valence and conduction bands lie very close in the Brillouin zone. The momenta where such local extrema occur are referred to as "valleys". There has been growing interest in materials where several of such valleys exist in the first Brillouin zone, as they provide a new effective degree of freedom, in addition to conventional charge and spin. The technology of control over valley degrees of freedom is referred to as valleytronics, analogous to spintronics where the spin degree of freedom is manipulated. In a two-dimensional (2D) honeycomb lattice, when the centrosymmetry ($\hat{P}$) is broken, the two inequivalent sublattices trigger a degenerate but inequivalent pair of valleys which are well separated in the 2D hexagonal Brillouin zone with suppressed intervalley interactions. For example, electrons in two valleys in 2D transition-metal dichalcogenides can be selectively excited by different circularly polarized light [1–3]. Resulting valleytronics [4] has potential application in the next-generation nanoelectronics devices to encode and manipulate information [5–11].

Other than the real space centrosymmetry $\hat{P}$, time-reversal symmetry $\hat{T}$ that is related to the spin also plays an important role in today's condensed-matter physics. For example, recently discovered topological insulators are protected by $\hat{T}$, which have dissipationless metallic surface or edge states and are robust against any kind of weak disorders [12]. A novel striking topological phenomenon, quantum anomalous Hall effect (QAHE), could arise when $\hat{T}$ is broken in a topological insulator [13–15]. The QAHE of an insulator is characterized by a nonzero topological invariant Chern number $C = \frac{1}{2\pi}\int \Omega(k) d^2k$, where $\Omega(k)$ is Berry curvature in the k-space [15].

It is more intriguing when both $\hat{T}$ and $\hat{P}$ are broken in a honeycomb lattice, which could lead to valley-polarized (VP-)QAHE. The VP-QAHE is characterized by two nonzero indices: the Chern number C (=C_K+$C_{K'}$) and valley Chern number C_v (=C_K–$C_{K'}$), where K and K' are the two valleys of the honeycomb lattice. For example, in a pioneering model calculation, Pan *et al.* [16] showed that a strong extrinsic Rashba spin-orbit coupling (SOC) in silicene can trigger VP-QAHE with C = –1 and C_v = 3 (where intervalley interaction C_v drops to 1 and C remains –1). This property adds topology into

quantum valley Hall effect so that it provides the possibility to design and realize dissipationless valleytronics in a robust way. However, due to the stringent criteria, most studies are limited to toy model calculations and freestanding films [16–22]. It is highly desirable to search for VP-QAHE mechanism that is experimentally feasible in 2D materials supported by a substrate.

In this work, we propose a different mechanism to realize VP-QAHE in honeycomb lattice by introducing a staggered magnetic exchange field, which is an *intrinsic* property and can be easily realized in experiments. By applying a low energy $k{\cdot}p$ model, we develop a general phase diagram of band inversion at K and/or K' valley of the honeycomb lattice under intrinsic intra-atomic SOC effect. We show that VP-QAHE can be expected when the two sublattices (denoted as A and B) are experiencing strongly different exchange field rather than strong Rashba SOC [Fig. 1(a)]. Most remarkably, based on first-principles calculation, we show that such VP-QAHE can be realized in a Co decorated In adlayer that is epitaxially grown on a Si(111)-(2×2) reconstructed surface. The advances in epitaxial growth of heavy atomic layers and surface alloying techniques on the Si(111) surface have shown the potential to synthesize such a structure. Specifically, the epitaxially grown In-adlayer forms stable triangular clusters on a Si(111)-(2×2) reconstructed surface, as observed in previous experiments [23–25] and demonstrated in subsequent theoretical calculations [26,27]. We show that this system can be viewed as a ferrimagnetic (FIM) honeycomb lattice, which has a band inversion at K, consistent with our model. By integrating Berry curvature, we obtain $C_K = -1$ and $C_{K'} = 0$, hence $C = C_v = -1$.

We start with a four-band $k{\cdot}p$ model around the K and K' valleys to first order in k. The Hamiltonian can be written as,

$$\hat{H}_0 = v_{\mathrm{F}}\left(\tau\hat{\sigma}_x k_x + \hat{\sigma}_y k_y\right)\hat{s}_0 - m_{\mathrm{A}}\frac{\hat{\sigma}_z + \hat{\sigma}_0}{2}\hat{s}_z - m_{\mathrm{B}}\frac{\hat{\sigma}_0 - \hat{\sigma}_z}{2}\hat{s}_z + \frac{\delta}{2}\hat{\sigma}_z\hat{s}_0\,, \qquad (1)$$

where σ_i and s_i (i=0,x,y,z) are Pauli matrices for sublattice and spin degrees of freedom, respectively. v_{F} is Fermi velocity at the valley, and τ=±1 denotes the valley index. The first term is the graphene-like band dispersion [28]. The second and third terms describe the staggered exchange field on the two sublattices that simultaneously break $\hat{T}$ and $\hat{P}$.

Without loss of generality, we assume that $m_A > 0$ and $|m_A| > |m_B|$. We also include the on-site energy difference between the two sublattices (δ). Here, we only consider the case when δ is small ($|\delta| < |m_A| - |m_B|$), because very large δ always yields large band gap with trivial topology. Note that the specified value of δ does not change the main physics here, even when $\delta = 0$.

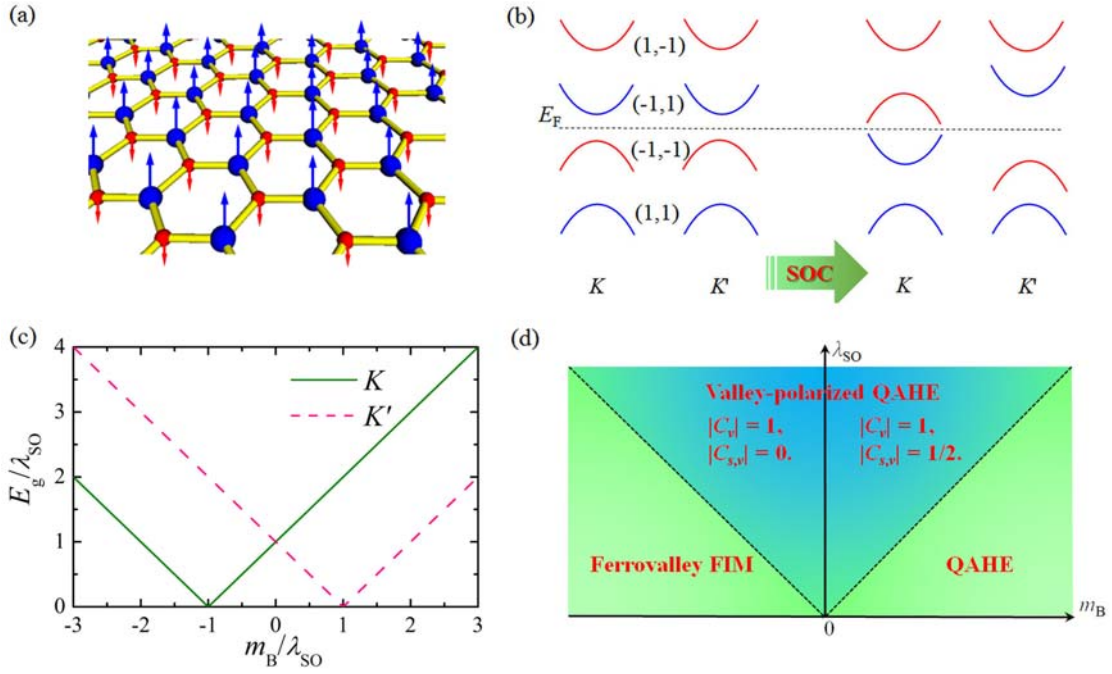

FIG. 1. (a) Ferrimagnetic honeycomb lattice (blue: sublattice-A, spin-up; red: sublattice-B, spin-down). (b) Schematic plot of low energy band at two valleys before (left panel) and after (right panel) including atomic SOC. The index in the left panel is $(\langle\sigma_z\rangle, \langle s_z\rangle)$ of each band at the valley. (c) Variation of band gap at the two valleys E_g/λ_{SO} with respect to m_B/λ_{SO}. (d) Topological phase diagram of m_B and λ_{SO} (the dashed line is $\lambda_{SO} = |m_B|$).

The solution of the above Hamiltonian yields four spin polarized bands that can be denoted by a pair index $(\langle\sigma_z\rangle, \langle s_z\rangle)$ at the valleys. In the left panel of Fig. 1(b) we plot a schematic band for FIM honeycomb lattice ($m_B < 0$). When $m_B > 0$, the (–1, 1) and (–1, –1) bands exchange their energy sequence around the Fermi level, which corresponds to an already inverted band order at two valleys. Because m_A is larger than m_B, the central two bands mainly belong to sublattice-B, i.e. $\langle\sigma_z\rangle = -1$. Hence, for simplicity we only apply

intrinsic SOC effect on them. The *ad hoc* intrinsic SOC effect is given by [3,8] (we will show below that this is the intra-atomic **L**·**S** form in our material),

$$\hat{H}_{\mathrm{SO}} = -\lambda_{\mathrm{SO}}\tau\frac{\hat{\sigma}_0 - \hat{\sigma}_z}{2}\hat{s}_z, \tag{2}$$

where $\lambda_{\mathrm{SO}} > 0$ is the SOC coefficient. Under basis set $[\Psi_{A\uparrow},\Psi_{A\downarrow},\Psi_{B\uparrow},\Psi_{B\downarrow}]^{\mathrm{T}}$, we obtain the energy spectra

$$\begin{aligned} E_{\uparrow} &= \frac{1}{2}\left[\left(m_{\mathrm{A}} + m_{\mathrm{B}} + \tau\lambda_{\mathrm{SO}}\right) \pm \sqrt{\left(m_{\mathrm{A}} - m_{\mathrm{B}} + \delta - \tau\lambda_{\mathrm{SO}}\right)^2 + 4v_{\mathrm{F}}^2k^2}\right] \\ E_{\downarrow} &= \frac{1}{2}\left[-\left(m_{\mathrm{A}} + m_{\mathrm{B}} + \tau\lambda_{\mathrm{SO}}\right) \pm \sqrt{\left(m_{\mathrm{A}} - m_{\mathrm{B}} - \delta - \tau\lambda_{\mathrm{SO}}\right)^2 + 4v_{\mathrm{F}}^2k^2}\right] \end{aligned}. \tag{3}$$

This implies that the SOC decreases (increases) the spin-up (down) band energy at the *K* valley, while it moves the spin-up (down) band in higher (lower) energy at *K′*. The energy gap, E_{g}, between the valence and conduction bands is plotted in Fig. 1(c) as a function of $m_{\mathrm{B}}/\lambda_{\mathrm{SO}}$. For the FIM system ($m_{\mathrm{B}} < 0$), both valleys are topologically trivial when $\lambda_{\mathrm{SO}} < |m_{\mathrm{B}}|$, but their band gaps are different. This corresponds to a ferrovalley state that has been recently proposed in a freestanding magnetic 2*H*-VSe_2 monolayer [29]. As λ_{SO} increases, the band gap at *K* valley closes and re-opens when $\lambda_{\mathrm{SO}} > |m_{\mathrm{B}}|$ and the *K′* valley remains semiconducting. The schematic band is plotted in the right panel of Fig. 1(b). The valence band below the Fermi level shows a skyrmion spin texture, i.e., it points along the +*z* direction (spin-up) at *K* and gradually and isotropically flips to spin-down away from *K*. This corresponds to a nonzero topological index and the system would show VP-QAHE. When $m_{\mathrm{B}} > 0$, small SOC ($\lambda_{\mathrm{SO}} < m_{\mathrm{B}}$) does not change the band inversion feature in both *K* and *K′* valleys, which is a ferro-valleytronic QAHE. Large SOC ($\lambda_{\mathrm{SO}} > m_{\mathrm{B}} > 0$) flip back the two bands at *K′*, which also yields a VP-QAHE (actually it is different from the FIM case because it also has a spin Chern number of ~1/2 at *K′*, as discussed in hetero-functionalized Sb-monolayer [30]). Based on these band order analyses, we plot a topological phase diagram in Fig. 1(d). Note that in all these discussions, a strong Rashba SOC is not included. However, a Rashba SOC (induced by centrosymmetry broken) $\widehat{H}_R = \tau\sigma_z a\lambda_R\left(k_y s_x - k_x s_y\right)$ [31] is still necessary which would open a finite band gap at

$$v_{\mathrm{F}}\left|k_{\Delta}\right|=\sqrt{\left(m_{\mathrm{A}}-m_{\mathrm{B}}-\lambda_{\mathrm{SO}}\right)\left(m_{\mathrm{B}}+\lambda_{\mathrm{SO}}\right)-\frac{\delta^{2}\left(m_{\mathrm{B}}+\lambda_{\mathrm{SO}}\right)}{m_{\mathrm{A}}-m_{\mathrm{B}}-\lambda_{\mathrm{SO}}}}, \tag{4}$$

between the spin-up and spin-down bands and yield an insulating property with band gap (according to degenerate perturbation method) of

$$E_{g}\approx 2\frac{a\lambda_{\mathrm{R}}}{v_{\mathrm{F}}}\left[m_{\mathrm{A}}+m_{\mathrm{B}}+\lambda_{\mathrm{SO}}+\Delta+\frac{2\left(m_{\mathrm{A}}-m_{\mathrm{B}}-\lambda_{\mathrm{SO}}\right)\left(m_{\mathrm{B}}+\lambda_{\mathrm{SO}}\right)}{m_{\mathrm{A}}-m_{\mathrm{B}}+\Delta-\lambda_{\mathrm{SO}}}\right]. \tag{5}$$

After establishing the staggered exchange field induced VP-QAHE phase diagram, we carry out first-principles calculations [32–41] to show that it is achievable in a real material. Instead of focusing on a freestanding thin film which is difficult to synthesize experimentally and whose topology may vary when depositing on a substrate, we explore a 2D system supported on a substrate [42,43]. Owing to the experimental success of epitaxial growth of In-triangle on a Si(111)-(2×2) surface [24–28], we predict that it has the potential to realize VP-QAHE, once decorated with magnetic Co.

Figure 2(a) shows the optimized ground state of Co decorated In-triangle adlayer on a Si(111)-(2×2) reconstructed surface. Similar to previous experimental and theoretical works [24–28], three In atoms cluster together to form a triangle. The relaxed In-In bond length is 3.11 Å. Each In is bonded with two substrate Si atoms, with In-Si bond length of 2.98 Å. The Co atom saturates the remaining vertical Si dangling bond that connects the triangular In cluster, with the optimized Co-In and Co-Si bond lengths of 2.64 and 2.39 Å, respectively. The binding energy of the Co atom, calculated as $E_b = E_{\mathrm{Co}} + E_{\mathrm{In@Si}} - E_{\mathrm{CoIn@Si}}$, is 2.94 eV. Here, E_{Co}, $E_{\mathrm{In@Si}}$, and $E_{\mathrm{CoIn@Si}}$ are the total energies of a single Co atom, In-triangle adsorbed on Si, and the whole system, respectively. This is larger than when an In atom is adsorbed on the same position (2.64 eV) as in experiments, indicating that the structure is experimentally feasible by surface alloying or epitaxial growth technique. Note that the 2D deposition pattern of the In-triangle and Co atom forms a perfect honeycomb lattice, as its layer symmetry group is *P*3*m*1.

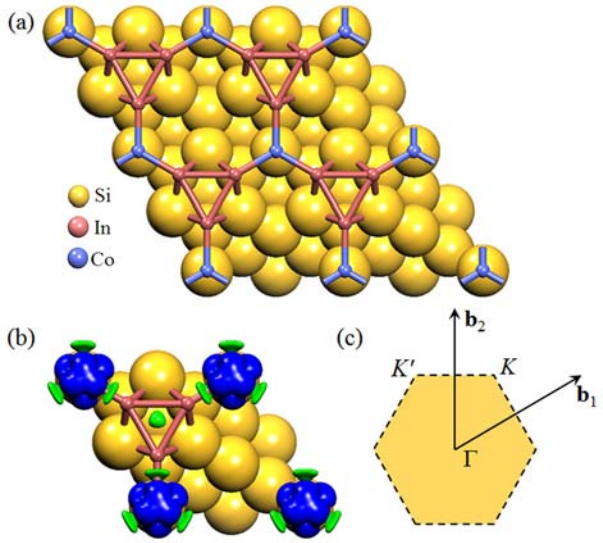

FIG. 2. (a) The atomic structure of Co decorated In-triangle adlayer on Si. (b) Iso-surface (0.005 $|e|/\text{Å}^3$) of spin density with blue and green colors representing up and down spins, respectively. (c) The first Brillouin zone.

For a bare Si(111)-(2×2) surface, there are four Si atoms with unpaired p_z orbitals. Each In atom has three valence electrons, where two of them form In-In bond and the other one saturates the Si-p_z to form In-Si bond. Therefore, the Si substrate only needs one more electron to be stable and semiconducting. The adsorbed Co contributes that electron with eight valence electrons left. Due to the Hund's rule, these eight electrons fill five spin-up and three spin-down orbitals, resulting in net magnetic moments of 2 μ_B. These analyses agree well with our DFT results: the Co carries 2.01 μ_B local magnetic moment. From the spin density distribution [Fig. 2(b)] we see that the magnetism mainly comes from the d_{xz} and d_{yz} orbitals, with a small portion coming from d_z^2 due to hybridization with Si-p_z. In addition, the In-triangle is slightly spin polarized, carrying –0.13 μ_B magnetic moment. Interestingly, the spin-down electrons of In-triangle are localized at the center, rather than on the In atomic sites. This will be discussed later. Such spin density wave shows a well-defined FIM honeycomb pattern.

The calculated band structure along high symmetry k-path [Fig. 2(c)] shows a direct semiconducting feature with a small band gap (~16 meV) [32], similar to that in Fig. 1(b). The Si(111) substrate opens a large band gap near the Fermi level, consistent with the

above analysis. The two valleys K and K' show similar behavior. Hence, we only discuss the K valley in the following. Near the K valley, the valence band (VB) and conduction band (CB) belong to spin-down and spin-up channels, respectively. The VB–1 and CB+1 are in the spin-up and spin-down channels, respectively. Next, we focus on their orbital contribution. By calculating the band-decomposed charge of these four bands at K, we find that the orbital contribution of VB and CB are the same – mainly from the center of the In-triangle. To be specific, they arise from the In-p_x,p_y electrons. Similarly, the orbital contribution of VB–1 and CB+1 are the same. They come from the hybridization between Co-d_z^2 and the p_z electron of the Si that resides beneath Co. All of these features agree well with our model [left panel of Fig. 1(b)] when one takes Co as sublattice-A and the whole In-triangle as sublattice-B.

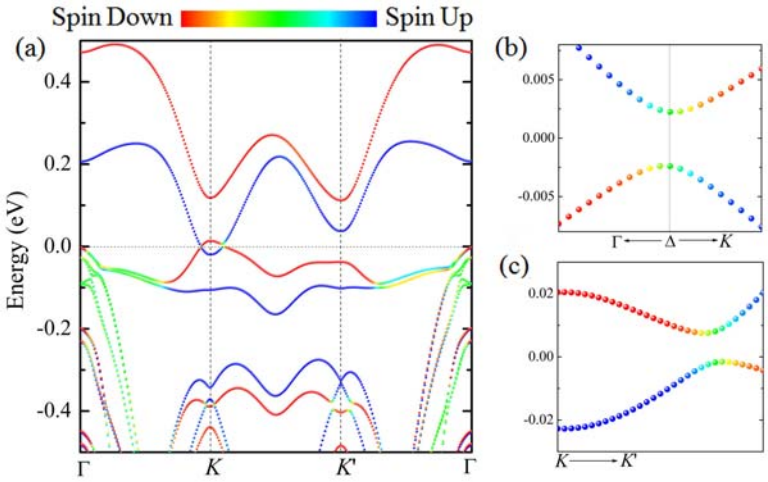

FIG. 3. (a) Band structure (with SOC) with color of each state representing out-of-plane $\langle s_z \rangle$. (b) and (c) are zoom-in plot of band structure near the Fermi level along the $\Gamma \rightarrow K$ and $K \rightarrow K'$ paths, respectively. In (b) Δ denotes the point with narrowest band gap.

The SOC effect lifts the degeneracy between the two valleys. From Fig. 3(a) we find that consistent with our model [right panel of Fig. 1(b)], the original spin-up CB at K moves downward and lies below the spin-down VB at K (band inversion). We plot a 3D spin texture of this new valence band around the K valley [32], which shows a spiral skyrmion texture, consistent with the model. The band energy difference between them (at K) is 41 meV. On the contrary, the K' valley remains to be trivially semiconducting

with band gap of 76 meV. We observe that most states around the two valleys have large out-of-plane spin texture, indicating weak Rashba effect [44,45]. The global band gap is determined near K valley. As shown in the zoom-in plot [Figs. 3(b) and 3(c)], the global band gap is ~5 meV along the $\Gamma \rightarrow K$ path. Note that this band gap can be furthermore increased by applying an electric field and using heavier Tl atom instead of In [32]. By fitting the model parameters with our first-principles results we obtain that m_A = 109.7 meV, m_B = –7.3 meV, δ = 3.6 meV, and λ_{SO} = 27.3 meV. The large positive m_A and small negative m_B values also agree with the FIM spin density.

Now we explore the reason why the In-triangle only contributes one electron to the low energy bands. The little group of the valley includes three-fold rotation C_3 and the two valleys are related by mirror reflection. For the In-triangle, the In-p_z orbitals are saturated by the substrate Si so that the basis function forming the three In-In bonds are $|\varphi_{\mathrm{In}}^{\tau}\rangle = \frac{1}{\sqrt{2}}\left(|p_x\rangle + i\tau|p_y\rangle\right)$. The nearest neighbor hopping t_{In} among them yields its local Hamiltonian,

$$\hat{H}_{\mathrm{In}} = t_{\mathrm{In}} \begin{pmatrix} 0 & 1 & 1 \\ 1 & 0 & 1 \\ 1 & 1 & 0 \end{pmatrix}. \tag{6}$$

By symmetrizing it, we obtain the eigenvalues and their corresponding eigenstates,

$$\begin{aligned} &\varepsilon_1 = 2t_{\mathrm{In}}, \qquad \psi_1 = \frac{1}{\sqrt{3}}[1,1,1]^{\mathrm{T}}; \\ &\varepsilon_{2,3} = -t_{\mathrm{In}}, \quad \psi_2 = \frac{1}{\sqrt{2}}[1,0,-1]^{\mathrm{T}}, \quad \psi_3 = \frac{1}{\sqrt{6}}[1,-2,1]^{\mathrm{T}} \end{aligned} \tag{7}$$

The eigenstate ψ_1 is perpendicular to the xy plane and resides at the triangle center. Its energy is higher than that of 5p_z orbital and is similar with Co-3d orbitals, giving small on-site energy difference δ. The degenerate ψ_2 and ψ_3 are energetically far lower from it [46]. Thus, the band structure of the whole system can be reduced to a honeycomb lattice. The intra-atomic SOC form under ψ_1 also yields Eq. (2).

We calculate the Berry curvature [47] from the first-principles wavefunction to explore its topology,

$$\Omega(k) = -\sum_{E_{nk} \le \mu} \sum_{m \ne n} \frac{2\,\mathrm{Im}\langle \psi_{nk} | \hat{v}_x | \psi_{mk} \rangle \langle \psi_{mk} | \hat{v}_y | \psi_{nk} \rangle}{(E_{nk} - E_{mk})^2}, \tag{8}$$

where μ is the chemical potential and $\hat{v}_{x,y}$ is the velocity operator. The calculated Berry curvature is shown in Figs. 4(a) and 4(b), where we observe a sharp negative peak in the vicinity of *K*, but very small around *K′*. From the 2D *k*-resolved Berry curvature the C_3 rotation is clearly seen. Integrating the Berry curvature over the 2D *k*-space gives the Chern number $C = -1$. Actually, the integrations in triangular regions centered at *K* and *K′* valleys whose area equal to half of the first Brillouin zone give $C_K = -1$ and $C_{K'} = 0$. Thus, the valley Chern number $C_v = -1$. This confirms the topological feature of our FIM VP-QAHE model. The integrated spin Chern number is zero, which also agrees with our model.

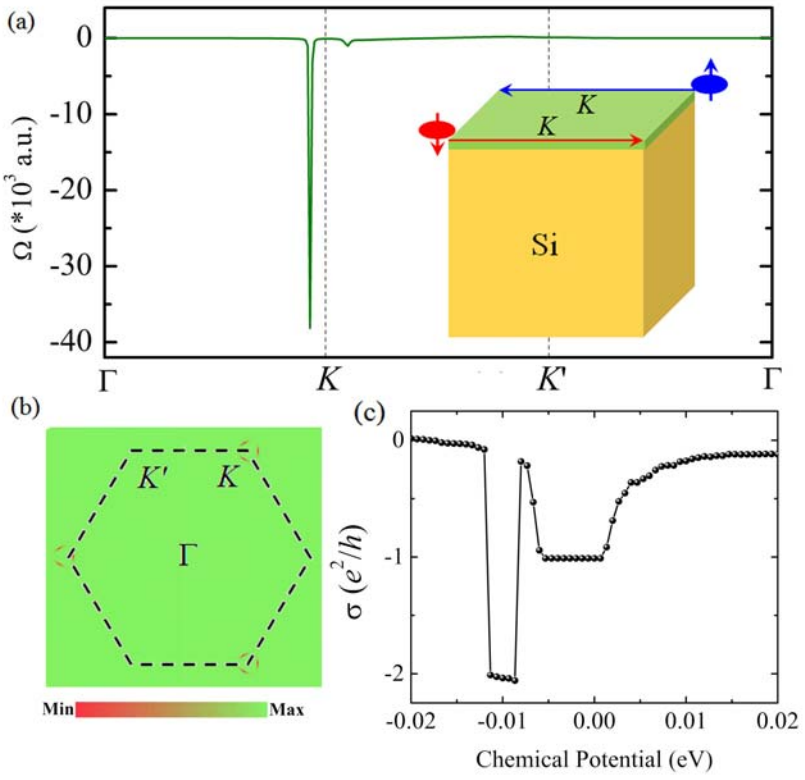

FIG. 4. (a) Berry curvature along the high symmetry *k*-path. (Inset) Schematic plot of VP-QAHE with their edge conductance. (b) *k*-resolved Berry curvature. (c) Anomalous Hall conductance variation of chemical potential.

By varying the chemical potential, we calculate the anomalous Hall conductance $\sigma = C \cdot e^2/h$. As shown in Fig. 4(c), a clear plateau of $\sigma = -e^2/h$ can be observed around the Fermi level, and it increases back to small value as chemical potential lies outside the band gap. The nearly flat terrace of $\sigma \sim -2e^2/h$ at $\mu \sim -0.01$ eV is attributed to band inversion around the Γ, which arises from the Zeeman splitting and is not protected topologically.

In general, a topological property is robust and stable against any kind of sufficiently weak disorder [12,15,22]. In our calculations, the structure, based on the experimental observation, is well-ordered. Thus, the two valleys are well separated and intervalley scattering is absent. In the presence of short-range disorder, invervalley scattering would appear. Especially, when the periodicity is increased to ($3n \times 3n$) where n is an integer, the valleys K and K' are folded into the Γ point, resulting in a significantly enhanced intervalley interaction. However, while the K valley has a spin-polarized metallic edge state ($C_K = -1$), the K' valley is insulating when the system is cut into a 1D strip [inset of Fig. 4(a)]. Thus, the back scattering is suppressed and VP-QAHE is expected under weak short-range disorders. In addition, a previous study showed that random distribution of adatoms on a honeycomb lattice (which induce magnetization and SOC) can weaken the intervalley scattering, but the magnetization and SOC are not affected. The topological features (QSHE and QAHE) still remain [48]. Therefore, in our case, we expect that neither weak disorder nor small perturbations will affect its topology.

In summary, we predict a VP-QAHE mechanism by introducing a staggered magnetic exchange field to the honeycomb lattice model, which can be easily achieved in real materials. Furthermore, we suggest a feasible material realization of this model in the Co decorated In-triangle adlayer supported on Si(111)-(2×2) substrate, which can be reduced to a FIM honeycomb lattice. The QAHE only occurs at the K valley, while the K' valley remains normal insulating. Compared with previous model studies on silicene sheet [16,17], the current strategy does not need a strong Rashba effect. The substrate supported FIM adlayer is experimentally more feasible than the freestanding half-hydrogenated Bi bilayers [20]. From the model point of view, the half-hydrogenated Bi

bilayer lies near the $m_B = 0$ line in Fig. 1(d). Our results not only enrich the basic understanding of VP-QAHE phase, but also extend such phenomenon from freestanding model discussion to substrate-supported real materials. This substrate-supported collinear FIM material also holds potential to realize fascinating VP-spin Nernst effect [49].

Acknowledgments. This work is partially supported by grants from the U.S. Department of Energy, Office of Basic Energy Sciences, Division of Materials Sciences and Engineering (No. DE-FG02-96ER45579), the National Natural Science Foundation of China (No. 21573008) and the National Key Research and Development Program of China (Grant 2016YFB0100200). Resources of the National Energy Research Scientific Computing Center supported by the Office of Science of the U.S. Department of Energy under Contract no. DE-AC02-05CH11231 is also acknowledged.

*jzhou2@vcu.edu

†pjena@vcu.edu

References:

[1] K. Mak, K. He, J. Shan, and T. F. Heinz, Control of valley polarization in monolayer MoS_2 by optical helicity. Nat. Nanotechnol. **7**, 494 (2012).

[2] T. Cao, G. Wang, W. Han, H. Ye, C. Zhu, J. Shi, Q. Niu, P. Tan, E. Wang, B. Liu, and J. Feng, Valley-selective circular dichroism of monolayer molybdenum disulphide. Nat. Commun. **3**, 887 (2012).

[3] D. Xiao, G.-B. Liu, W. Feng, X. Xu, and W. Yao, Coupled Spin and Valley Physics in Monolayers of MoS_2 and Other Group-VI Dichalcogenides. Phys. Rev. Lett. **108**, 196802 (2012).

[4] D. Pesin and A. H. MacDonald, Spintronics and pseudospintronics in graphene and topological insulators. Nat. Mater. **11**, 409 (2012).

[5] A. Rycerz, J. Tworzydlo, and C. W. J. Beenakker, Valley filter and valley valve in graphene. Nat. Phys. **3**, 172 (2007).

[6] Q. Liu, X. Zhang, and A. Zunger, Intrinsic Circular Polarization in Centrosymmetric Stacks of Transition-Metal Dichalcogenide Compounds. Phys. Rev. Lett. **114**, 087402 (2015).

[7] D. Xiao, W. Yao, and Q. Niu, Valley-Contrasting Physics in Graphene: Magnetic Moment and Topological Transport. Phys. Rev. Lett. **99**, 236809 (2007).

[8] X. Li, T. Cao, Q. Niu, J. Shi, and J. Feng, Coupling the valley degree of freedom to antiferromagnetic order. Proc. Natl. Acad. Sci. U.S.A. **110**, 3738 (2013).

[9] H.-J. Kim, C. Li, J. Feng, J.-H. Cho, Z. Zhang, Competing magnetic orderings and tunable topological states in two-dimensional hexagonal organometallic lattices. Phys. Rev. B **93**, 041404(R) (2016).

[10] F. Zhang, A. H. MacDonald, and E. J. Mele, Valley Chern numbers and boundary modes in gapped bilayer graphene. Proc. Natl. Acad. Sci. U.S.A. **110**, 10546 (2013).

[11] J. Zhou, C. Huang, E. Kan, and P. Jena, Valley contrasting in epitaxial growth of In/Tl homoatomic monolayer with anomalous Nernst conductance. Phys. Rev. B **94**, 035151 (2016).

[12] M. Z. Hasan and C. L. Kane, *Colloquium*: Topological insulators. Rev. Mod. Phys. **82**, 3045 (2010).

[13] F. D. M. Haldane, Model for a Quantum Hall Effect without Landau Levels: Condensed-Matter Realization of the "Parity Anomaly". Phys. Rev. Lett. **61**, 2015 (1988).

[14] R. Yu, W. Zhang, H.-J. Zhang, S.-C. Zhang, X. Dai, and Z. Fang, Quantized Anomalous Hall Effect in Magnetic Topological Insulators. Science **329**, 5987 (2010); C.-Z. Chang, J. Zhang, X. Feng, J. Shen, Z. Zhang, M. Guo, K. Li, Y. Ou, P. Wei, L.-L. Wang, *et al.* Experimental Observation of the Quantum Anomalous Hall Effect in a Magnetic Topological Insulator. Science **340**, 167 (2013).

[15] H. Weng, R. Yu, X. Hu, X. Dai, and Z. Fang, Quantum anomalous Hall effect and related topological electronic states. Adv. Phys. **64**, 227 (2015).

[16] H. Pan, Z. Li, C.-C. Liu, G. Zhu, Z. Qiao, and Y. Yao, Valley-Polarized Quantum Anomalous Hall Effect in Silicene. Phys. Rev. Lett. **112**, 106802 (2014).

[17] Z. Yu, H. Pan, and Y. Yao, Electric field controlled spin- and valley-polarized edge states in silicene with extrinsic Rashba effect. Phys. Rev. B **92**, 155419 (2015).

[18] H. Pan, X. Li, H. Jiang, Y. Yao, and S. A. Yang, Valley-polarized quantum anomalous Hall phase and disorder-induced valley-filtered chiral edge channels. Phys. Rev. B **91**, 045404 (2015).

[19] H. Pan, X. Li, F. Zhang, and S. A. Yang, Perfect valley filter in a topological domain wall. Phys. Rev. B **92**, 041404(R) (2015).

[20] C.-C. Liu, J.-J. Zhou, and Y. Yao, Valley-polarized quantum anomalous Hall phases and tunable topological phase transitions in half-hydrogenated Bi honeycomb monolayers. Phys. Rev. B **91**, 165430 (2015).

[21] C. Niu, G. Bihlmayer, H. Zhang, D. Wortmann, S. Blügel, and Y. Mokrousov, Functionalized bismuth films: Giant gap quantum spin Hall and valley-polarized quantum anomalous Hall states. Phys. Rev. B **91**, 041303(R) (2015).

[22] Y. Ren, Z. Qiao, and Q. Niu, Topological phases in two-dimensional materials: a review. Rep. Prog. Phys. **79**, 066501 (2016).

[23] A. A. Saranin, T. Numata, O. Kubo, M. Katayama, and K. Oura, Structural transformations of the Si(111) 2×2-In surface induced by STM tip and thermal annealing. Appl. Surf. Sci. **121-122**, 183 (1997).

[24] D. V. Gruznev, A. V. Matetskiy, I. V. Gvozd, A. V. Zotov, and A. A. Saranin, C_{60} adsorption onto the one-atomic-layer In films on Si(111) surface. Surf. Sci. **605**, 1951 (2011).

[25] A. A. Saranin, T. Numata, O. Kubo, H. Tani, M. Katayama, V. G. Lifshits, and K. Oura, STM tip-induced diffusion of In atoms on the Si(111)$\sqrt{3}\times\sqrt{3}$-In surface. Phys. Rev. B **56**, 7449 (1997).

[26] J. P. Chou, C. M. Wei, Y. L. Wang, D. V. Gruznev, L. V. Bondarenko, A. V. Matetskiy, A. Y. Tupchaya, A. V. Zotov, and A. A. Saranin, Atomic structure and electronic properties of the In/Si(111) 2×2 surface. Phys. Rev. B **89**, 155310 (2014).

[27] S. G. Kwon and M. H. Kang, Honeycomb network of indium trimers and monomers on Si(111)-(2×2). Phys. Rev. B **89**, 165304 (2014).

[28] C. L. Kane and E. J. Mele, Quantum Spin Hall Effect in Graphene. Phys. Rev. Lett. **95**, 226801 (2005).

[29] W.-Y. Tong, S.-J. Gong, X. Wan, and C.-G. Duan, Concepts of ferrovalley material and anomalous valley Hall effect. Nat. Commun. **7**, 13612 (2016).

[30] T. Zhou, J. Zhang, B. Zhao, H. Zhang, and Z. Yang, Quantum Spin-Quantum Anomalous Hall Insulators and Topological Transitions in Functionalized Sb(111) Monolayers. Nano Lett. **15**, 5149 (2015).

[31] M. Ezawa, Valley-Polarized Metals and Quantum Anomalous Hall Effect in Silicene. Phys. Rev. Lett. **109**, 055502 (2012).

[32] Supplemental Material for computational details, different decorating configurations and their relative energies, band structure without SOC and orbital contribution, valence band spin texture around the *K* valley, and modulation of band gap details, which includes Refs. [33–41].

[33] J. P. Perdew, K. Burke, and M. Ernzerhof, Generalized Gradient Approximation Made Simple. Phys. Rev. Lett. **77**, 3865 (1996).

[34] G. Kresse and J. Furthmüller, Efficient iterative schemes for *ab initio* total-energy calculations using a plane-wave basis set. Phys. Rev. B **54**, 11169 (1996).

[35] P. E. Blöchl, Projector augmented-wave method. Phys. Rev. B **50**, 17953 (1994).

[36] J. Zhou and Q. Sun, Magnetism of Phthalocyanine-Based Organometallic Single Porous Sheet. J. Am. Chem. Soc. **133**, 15113 (2011).

[37] T. P. Kaloni, N. Singh, and U. Schwingenschlögl, Prediction of a quantum anomalous Hall state in Co-decorated silicene. Phys. Rev. B **89**, 035409 (2014).

[38] L. Wang, T. Maxisch, and G. Ceder, Oxidation energies of transition metal oxides within the GGA+*U* framework. Phys. Rev. B **73**, 195107 (2006).

[39] V. Singh, M. Kosa, K. Majhi, and D. T. Major, Putting DFT to the Test: A First-Principles Study of Electronic, Magnetic, and Optical Properties of Co_3O_4. J. Chem. Theory Comput. **11**, 64 (2015).

[40] S. L. Dudarev, G. A. Botton, S. Y. Savrasov, C. J. Humphreys, and A. P. Sutton, Electron-energy-loss spectra and the structural stability of nickel oxide: An LSDA+*U* study. Phys. Rev. B **57**, 1505 (1998).

[41] H. J. Monkhorst and J. D. Pack, Special points for Brillouin-zone integrations. Phys. Rev. B **13**, 5188 (1976).

[42] M. Zhou, W. Ming, Z. Liu, Z. Wang, P. Li, and F. Liu, Epitaxial growth of large-gap quantum spin Hall insulator on semiconductor surface. Proc. Natl. Acad. Sci. U.S.A. **111**, 14378 (2014).

[43] B. Huang, K.-H. Jin, H. L. Zhuang, L. Zhang, and F. Liu, Interface orbital engineering of large-gap topological states: Decorating gold on a Si(111) surface. Phys. Rev. B **93**, 115117 (2016).

[44] Z. Qiao, H. Jiang, X. Li, Y. Yao, and Q. Niu, Microscopic theory of quantum anomalous Hall effect in graphene. Phys. Rev. B **85**, 115439 (2012).

[45] J. Zhou, Q. Sun, Q. Wang, Y. Kawazoe, and P. Jena, Intrinsic quantum spin Hall and anomalous Hall effects in *h*-Sb/Bi epitaxial growth on a ferromagnetic MnO_2 thin film. Nanoscale **8**, 11202 (2016).

[46] Z. Liu, Z.-F. Wang, J.-W. Mei, Y.-S. Wu, and F. Liu, Flat Chern Band in a Two-Dimensional Organometallic Framework. Phys. Rev. Lett. **110**, 106804 (2013).

[47] Y. G. Yao, L. Kleinman, A. H. MacDonald, J. Sinova, T. Jungwirth, D.-S. Wang, E. Wang, and Q. Niu, First Principles Calculation of Anomalous Hall Conductivity in Ferromagnetic bcc Fe. Phys. Rev. Lett. **92**, 037204 (2004).

[48] H. Jiang, Z. Qiao, H. Liu, J. Shi, and Q. Niu, Stabilizing Topological Phases in Graphene via Random Adsorption. Phys. Rev. Lett. **109**, 116803 (2012).

[49] R. Cheng, S. Okamoto, and D. Xiao, Spin Nernst Effect of Magnons in Collinear Antiferromagnets. Phys. Rev. Lett. **117**, 217202 (2016).